

SIMPLIFIED MODEL OF THE AIR FLOW ABOVE WAVES

V.N. Kudryavtsev

Marine Hydrophysical Institute, Sebastopol, Ukraine

V.K. Makin and J.F. Meirink

Royal Netherlands Meteorological Institute (KNMI), De Bilt, The Netherlands

1. Introduction

Physical phenomena that occur on the air-sea interface, are determined or strongly influenced by the air flow dynamics over the water waves. The exchange of momentum, heat, moisture and gases between the atmosphere and the ocean is determined to a large extent by the wind-wave interaction. A significant part of the momentum flux at the sea surface is formed directly by wind waves. Breaking waves could influence the exchange of heat and moisture by ejecting spray into the atmosphere. To account for this process, the vertical transport and spreading of spray, defined by the air flow above waves, should be known. Short wind waves, the key issue in remote sensing applications, are formed and modulated by the wind. To understand and parameterize the processes occurring at the sea surface and just above it, an explicit description of the air flow over waves is needed.

Starting from Miles (1957) numerous studies were dedicated to the problem (see, e.g., a review of Belcher and Hunt, 1998). Those studies brought the understanding that the modulation of the Reynolds stress close to the wave surface is responsible for the peculiarities of the wind-wave interaction. Belcher and Hunt (1993) distinguished two main regions above the waves: the inner and the outer region. In the inner region - a very thin region adjacent to the surface - the wave-induced turbulence is in local equilibrium with the local wind shear. In the outer region the turbulent stresses correlated with the wave surface are suppressed due to rapid distortion effects. Hence, the dynamics of the air flow corresponds to inviscid flow. The action of the Reynolds stress in the inner region causes a thickening of the stream lines on the forward slope of the wave. The inner region is thus asymmetric, leading to a pressure asymmetry in the outer region, which finally results in wave growth. The subdivision of the air flow into two regions considerably simplifies the analysis of the air flow dynamics above

waves. Belcher and Hunt (1993) found an analytical solution for the case of slowly moving waves (as compared to the wind velocity), while Cohen (1997) extended the theory for the case of fast moving waves. Harris et al. (1996) developed an eddy-viscosity model, in which the turbulent stresses in the inner region are parameterized by using the eddy-viscosity derived from the balance between the turbulent kinetic energy (TKE) production and its dissipation. In the outer region the eddy-viscosity coefficient is damped exponentially, and the turbulent stresses vanish.

We present here a simplified model of the wave boundary layer (SWBL), which we view as a convenient tool for applied studies that require the detailed structure of the air flow above waves. As an example we mention the calculation of the stress modulation in a model of the modulation of short waves by long waves (Kudryavtsev et al, 1997), or the calculation of the wave-induced velocity field for modelling sea spray distributions (Mestayer et al., 1996). The SWBL model can be useful to support experimental studies, both in the stage of preparation and measurements, when a quick decision to correct/extend measurements is needed, and the use of expensive numerical models of the wave boundary layer, like the model by Mastenbroek et al. (1996), is not feasible. The SWBL model describes the air flow above fast and slowly moving waves propagating at an arbitrary angle to the wind direction.

Following Belcher and Hunt (1993), by dividing the turbulent air flow into an outer and an inner region, the main simplification of the problem is achieved. In the outer region the wave-induced motion experiences an undulation typical for inviscid flow. The description of the outer region is further simplified by using the approximate solution of the Rayleigh equation for the vertical velocity suggested by Miles (1957) and Lighthill (1957). The amplitude of the vertical velocity is proportional to the mean velocity profile and decays exponentially with height. The horizontal velocity is found with the same accuracy from the vorticity conservation equation, once the vertical velocity is known.

In the inner region, the dynamics of the wave-induced motion is strongly affected by turbulent stresses. Towards the outer region, those are damped exponentially with height. Unlike Harris et al. (1996) who introduced damping of the eddy-viscosity coefficient, we apply damping directly on the stresses. The local eddy-viscosity closure scheme is used to parameterize the stresses. The eddy-viscosity coefficient is obtained from the balance between the turbulent kinetic energy production and its dissipation, where the dissipation is expressed in terms of the mixing length. The description of the inner region is based on the solution of the vorticity equation, in which the existence of the critical layer and the Reynolds stresses is accounted for. In Kudryavtsev et al. (1999) this

equation was solved analytically and explicit equations for the velocity and the shear stress were obtained. Here, for simplicity we solve the vorticity equation in the inner region numerically by iterations.

The solution of the simplified model is compared with the solution of the two-dimensional numerical wave boundary layer (2D WBL) model by Mastenbroek et al. (1996), based on a second-order Reynolds stress closure scheme. A good quantitative and qualitative agreement is found in velocity and stress distributions for fast and slow waves. The estimate of the growth rate parameter obtained by the SWBL model is consistent with the 2D WBL model. The results of the SWBL model are also compared with laboratory measurements of Hsu and Hsu (1983). The comparison is encouraging: the simplified model reproduces measurements of velocity and shear stress fields above waves as well as the 2D WBL numerical model. The main model assumption - the subdivision of the air flow into the outer and inner region - is supported by measurements.

2. Model equations

2.1. WAVE-INDUCED VARIATION OF WIND VELOCITY

A fully developed turbulent air flow over a monochromatic surface wave travelling on the (x_1, x_2) plane along the x_1 -axis with the phase speed c is considered. The air flow moves at an angle θ to the x_1 -axis, and all the air flow variables are uniform along the x_2 -axis. The surface is described by

$$\eta = \eta_o(kx_1 - \omega t),$$

where k and ω are the wavenumber and the frequency of the surface wave. In a frame of reference moving with the phase speed of the wave the equations governing the steady disturbances of the air flow caused by the wave are

$$u \frac{\partial u}{\partial x_1} + w \frac{\partial u}{\partial x_3} = -\frac{\partial}{\partial x_1}(p - \tau_{33}) + \frac{\partial}{\partial x_3}\tau_{13} + \frac{\partial}{\partial x_1}(\tau_{11} - \tau_{33}), \quad (1)$$

$$u \frac{\partial w}{\partial x_1} + w \frac{\partial w}{\partial x_3} = -\frac{\partial}{\partial x_3}(p - \tau_{33}) + \frac{\partial}{\partial x_1}\tau_{13}, \quad (2)$$

$$\frac{\partial}{\partial x_1}u + \frac{\partial}{\partial x_3}w = 0, \quad (3)$$

where p is pressure, τ_{13} is the Reynolds shear stress, and τ_{11} and τ_{33} are the Reynolds normal stresses.

In the wave-following coordinate system

$$\begin{aligned}x &= x_1, \\z &= x_3 - \eta(x_1, x_3),\end{aligned}\tag{4}$$

where $\eta(x_1, x_3) = \eta_0(x_1) \exp(-kx_3)$, equations (1)-(3) take the form

$$\begin{aligned}u\left(\frac{\partial}{\partial x} - \eta_1 \frac{\partial}{\partial z}\right)u + w(1 - \eta_3) \frac{\partial}{\partial z}u \\= -\left(\frac{\partial}{\partial x} - \eta_1 \frac{\partial}{\partial z}\right)P + (1 - \eta_3) \frac{\partial}{\partial z}\tau_{13} + \left(\frac{\partial}{\partial x} - \eta_1 \frac{\partial}{\partial z}\right)(\tau_{11} - \tau_{33}),\end{aligned}\tag{5}$$

$$\begin{aligned}u\left(\frac{\partial}{\partial x} - \eta_1 \frac{\partial}{\partial z}\right)w + w(1 - \eta_3) \frac{\partial}{\partial z}w = -(1 - \eta_3) \frac{\partial}{\partial z}P + \left(\frac{\partial}{\partial x} - \eta_1 \frac{\partial}{\partial z}\right)\tau_{13}, \\ \left(\frac{\partial}{\partial x} - \eta_1 \frac{\partial}{\partial z}\right)u + (1 - \eta_3) \frac{\partial}{\partial z}w = 0,\end{aligned}\tag{6}$$

where $P = p - \tau_{33}$, $\eta_1 = \partial\eta/\partial x_1$, and $\eta_3 = \partial\eta/\partial x_3$. The vertical transformation of the x_3 -coordinate is defined so that lines $z = \text{const.}$ are related to the streamlines of the irrotational flow over the wave.

The slope of the surface wave is assumed to be small, so that the air flow can be described as a sum of the basic flow and small perturbations

$$\begin{aligned}u(x, z) &= U(z) + \tilde{u}(x, z), \\v(x, z) &= V(z), \\w(x, z) &= \tilde{w}(x, z), \\P(x, z) &= \bar{P}(z) + \tilde{P}(x, z), \\\tau_{ij}(x, z) &= \bar{\tau}_{ij}(z) + \tilde{\tau}_{ij}(x, z).\end{aligned}\tag{8}$$

Here the wind velocity components U , V and the variables marked by the bar are related to the basic flow averaged over the x -coordinate, while the tilde refers to the perturbed flow. For a small air flow perturbation equations (5)-(7) can be linearized (hereafter the tilde over the perturbed variables is omitted) so that

$$U \frac{\partial u}{\partial x} + (w - \eta_1 U) \frac{\partial U}{\partial z} = -\frac{\partial P}{\partial x} + \frac{\partial \tau_{13}}{\partial z} + \frac{\partial}{\partial x}(\tau_{11} - \tau_{33}),\tag{9}$$

$$U \frac{\partial w}{\partial x} = -\frac{\partial P}{\partial z} + \frac{\partial \tau_{13}}{\partial x},\tag{10}$$

$$\frac{\partial u}{\partial x} + \frac{\partial}{\partial z}(w - \eta_1 U) = -\eta_{13} U,\tag{11}$$

where $\eta_{13} = \partial^2\eta/\partial x_1\partial x_3$. The mean wind velocity profile is assumed to vary logarithmically with height

$$\begin{aligned}U(z) &= (\bar{u}_*/\kappa) \ln(z/z_0) \cos \theta - c \\ &= (\bar{u}_*/\kappa) \ln(z/z_c) \cos \theta.\end{aligned}\tag{12}$$

Here κ is the von Karman constant, z_0 is the roughness parameter, \bar{u}_* is the friction velocity of the basic flow, and z_c is the critical height defined as

$$z_c = z_0 \exp\left(\frac{\kappa c}{\bar{u}_* \cos \theta}\right). \quad (13)$$

The roughness parameter is taken as the sum of the Charnock relation and the viscous roughness scale to account for low winds

$$z_0 = 0.014\bar{u}_*^2/g + 0.11\nu_a/\bar{u}_*, \quad (14)$$

where ν_a is the kinematic viscosity of the air.

The following boundary conditions are imposed:

$$u, w \rightarrow 0, \quad (15)$$

if $z \rightarrow \infty$, and

$$u = u_s, \quad (16)$$

$$w = -c \frac{\partial \eta_0}{\partial x} \quad (17)$$

at $z = z_0$, where u_s is the horizontal component of the surface wave orbital velocity.

The vorticity equation for the perturbed flow can be obtained from equations (9)-(11) by eliminating P

$$U \frac{\partial \Omega}{\partial x} + (w - \eta_1 U) U'' - \eta_{13} U U' = \left(\frac{\partial^2}{\partial z^2} - \frac{\partial^2}{\partial x^2}\right) \tau_{13} + \frac{\partial^2}{\partial x \partial z} (\tau_{11} - \tau_{33}), \quad (18)$$

where $\Omega = \partial u / \partial z - \partial w / \partial x$ is the vorticity, $U' = \partial U / \partial z$, and $U'' = \partial^2 U / \partial z^2$. The vorticity equation can be rewritten in the form of the Rayleigh equation for the vertical velocity using the continuity equation (11)

$$U \left(\frac{\partial^2 w}{\partial z^2} + \frac{\partial^2 w}{\partial x^2} \right) - w U'' = - \left(\frac{\partial^2}{\partial z^2} - \frac{\partial^2}{\partial x^2} \right) \tau_{13} - \frac{\partial^2}{\partial x \partial z} (\tau_{11} - \tau_{33}). \quad (19)$$

Equation (18) can be solved after the Reynolds stresses are expressed in terms of the independent variables, i.e. a turbulence closure scheme has to be introduced.

2.2. INNER AND OUTER REGIONS

Belcher and Hunt (1993) developed scaling arguments to describe how turbulence in the air flow is affected by the surface wave. They introduced two main time scales. The advection time scale, $T_D \sim k^{-1} / |U(z)|$,

characterizes the time for turbulent eddies to be advected and distorted by the mean flow over the wave. The eddy-turnover time scale, $T_L \sim \kappa z / \bar{u}_*$, characterizes the time for turbulent eddies to be adjusted to the local wind shear. The height at which these scales are comparable, $T_D \sim T_L$, is defined as the height of the inner region l . Belcher and Hunt (1993) estimated this height as

$$kl = \frac{2\kappa\bar{u}_*}{|U(l)|}. \quad (20)$$

In the case of very fast waves $kl = 2\kappa\bar{u}_*/c$. In the inner region (IR), defined as $z < l$, turbulence is in a local equilibrium with the local wind shear. In the outer region (OR), defined as $z > l$, turbulent eddies are advected too fast to be correlated with the local wind shear. The turbulent stresses are smeared out, i.e. they are not correlated with the surface wave, and the wave-induced air flow in the OR is largely inviscid.

The inner region has an important physical meaning. It is a thin region in the boundary layer above the wave where disturbances of turbulent stresses, caused by the interaction of the air flow with the surface, are located. Experimental evidence of the existence of the IR and the OR above waves was presented by Mastenbroek et al. (1996).

The height of the IR is the key parameter in the present model. Its height as a function of the inverse wave age parameter U_k/c (U_k is the wind speed at $z = k^{-1}$) is shown in Figure 1. For a given wind, the IR height increases with increasing phase speed of the wave and reaches its maximum in the vicinity of $U_k/c \sim 1$. This value of the inverse wave age parameter corresponds to waves at the peak of the wave spectrum of a fully developed sea. For faster waves the IR height decreases again.

The subdivision of the boundary layer above waves into an inner and an outer region allows considerable simplification of the parameterization of the Reynolds stresses. In the OR the turbulent stresses are simply neglected, and the air flow experiences inviscid undulation. In the IR a simple local eddy-viscosity scheme is used. In this region the air flow is strongly affected by wave-induced variations of the turbulent stresses. The boundary between the two regions is specified at height $h = nl$, where n is a constant of $O(1)$. At height $z = h$ the wind velocity and its vertical gradient are continuous.

2.3. CRITICAL LAYER

The critical layer plays a crucial role in quasi-laminar models of the air flow above waves (Miles, 1957). This type of models assume that

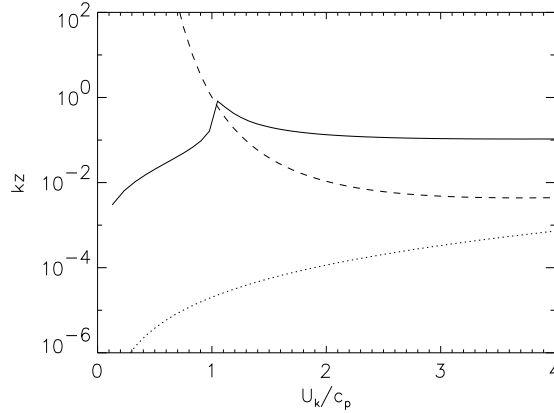


Figure 1. The vertical structure of the turbulent boundary layer over a wave as a function of U_k/c . The solid line is the IR scale kl , equation (20); the dashed line is the critical height kz_c , equation (13); the dotted line is the roughness scale kz_0 , equation (14).

the turbulent stresses can be neglected. In the terminology of the rapid distortion theory above waves this assumption is only valid when the height of the critical layer is situated in the outer region. The height z_c of the critical layer, defined by the condition $U(z_c) = 0$, equation (13), is shown in Figure 1. In the range of $U_k/c > 1$ the critical layer is located inside the inner region, so that turbulence should influence the dynamics of the critical layer.

Miles (1959) indicated that viscous effects become important and break the assumption of the quasi-laminar model when the viscous scale of the critical layer

$$\delta_c = \left(\frac{\nu_a \kappa z_c}{\bar{u}_* k} \right)^{1/3} \quad (21)$$

is of order z_c or more, i.e. $\delta_c \geq z_c$. If the critical layer is situated inside the IR, the eddy-viscosity takes the role of molecular viscosity in (21). In this case an estimate of the height δ_c can be obtained by replacing the viscosity ν_a in equation (21) by the eddy-viscosity $K = 2\kappa\bar{u}_*z$ at $z = z_c$ (see equation (44) below). Then equation (21) can be written as

$$\delta_c = (2\kappa^2 z_c^2 / k)^{1/3}, \quad (22)$$

and the condition $\delta_c \geq z_c$ is equivalent to

$$kz_c \leq 2\kappa^2.$$

It follows from Figure 1 that both conditions, $z_c < l$ and $kz_c \leq 2\kappa^2$, are satisfied in the range of $U_k/c > 1$. It means that in this range

turbulence dominates the dynamics of the air flow in the vicinity of the critical height. Hence, the applicability of the quasi-laminar model in the description of the air flow dynamics is restricted to a very narrow range of the inverse wave age parameter U_k/c around $U_k/c \simeq 1$.

3. Solution of equations

We assume that the wave steepness ak (a is the wave amplitude) is small. Hence, any air flow variable Y in the presence of waves experiences a small variation \tilde{Y} , which can be expanded in powers of ak

$$\tilde{Y}(x, z) = \langle Y \rangle (akY^{(1)}(x, z) + O(ak^2)), \quad (23)$$

where $\langle Y \rangle$ is a scale. To normalize the variation in the air flow parameters, u_*/κ is chosen as a scale for the wind velocities (including the mean wind speed), and \bar{u}_*^2 as a scale for the Reynolds stresses and pressure. The wave profile is introduced as the real part of

$$\eta_0(x) = ae^{ikx}. \quad (24)$$

The solution is then presented in the form of the normal mode

$$Y^{(1)}(x, z) = \hat{Y}(z)e^{ikx}, \quad (25)$$

where $\hat{Y}(z) = \hat{Y}_r(z) + i\hat{Y}_i(z)$ is the complex amplitude.

The second small parameter of the problem is the dimensionless height of the IR kl . As a variable \hat{Y} could depend on kl , we expand $\hat{Y}(z)$ in powers of kl

$$\hat{Y}(z) = \hat{Y}_0(z) + kl\hat{Y}_1(z) + O(k^2l^2). \quad (26)$$

The real part of $\hat{Y}(z)$ is the amplitude of the wave-induced variation in the air flow which is correlated with the wave elevation. The imaginary part of $\hat{Y}(z)$ is the amplitude of the variation which is correlated with the wave slope. Notice, that if $\hat{Y}_i(z)$ is positive then the maximum of the wave-induced variation is displaced towards the backward slope of the wave. As the surface wave is described by $\cos(kx)$, only the real part of (25) has a physical sense.

The analysis is done to first-order in ak (hereafter the superscript 1 is omitted), and to zero-order in kl (we shall call this solution the zero-order solution). For the vertical velocity the first order kl -correction of the zero-order solution has a significant physical sense (see Section 3.2.4), and will be considered additionally.

3.1. OUTER REGION

The turbulent stresses in the outer region are not correlated with the surface wave. Hence the wave-induced motion in the OR should be close to that of the inviscid air flow.

3.1.1. *Inviscid air flow*

When the air flow experiences inviscid undulation over the surface wave, equation (19) is reduced to the Rayleigh equation

$$U\left(\frac{\partial^2 \hat{w}_0}{\partial z^2} - k^2 \hat{w}_0\right) - \hat{w}_0 U'' = 0, \quad (27)$$

with the boundary conditions for the vertical velocity (15) and (17). This equation was studied in details in numerous papers starting from Miles (1957). Miles (1957) and Lighthill (1957) suggested an approximate solution of the Rayleigh equation in the form

$$\hat{w}_0(z) = \gamma U(z) \exp(-kz), \quad (28)$$

where γ is a constant of proportionality. As was mentioned by Phillips (1966), this constant should have a different value above and below the critical height. At $z < z_c$ the constant must be equal to i to satisfy the boundary condition (17). At $z > z_c$ the constant should differ from i due to the expected influence of the critical layer. A direct substitution of (28) into equation (27) shows that this solution satisfies the Rayleigh equation with the accuracy of $(kz \ln(kz/kz_c))^{-1}$ at large distance from the surface ($kz \sim 1$), and with the accuracy of kz close to the surface ($kz \ll 1$).

In Figure 2, the approximate solution (28) is compared with a numerical solution of the Rayleigh equation (27) for the inverse wave age parameter $U_{10}/c = 5$ and 2. To fit (28) to the numerical solution, the tuning constant γ is chosen as

$$\gamma = i, \text{ if } z < z_c, \quad (29)$$

$$\gamma = \frac{1}{2}(1 + i), \text{ if } z > z_c. \quad (30)$$

This choice gives a reasonable agreement between the approximate solution (28) and the numerical solution. Notice, that at the critical height equation (28) gives $\hat{w}_{0r}(z_c) = 0$. However, in fact $\hat{w}_{0r}(z_c)$ is slightly positive. Its value defines the energy transfer from the shear flow to waves in the quasi-laminar theory of Miles (1957). Miles (1957) estimated the magnitude of the vertical velocity at the critical height through the approximate solution (28) by integrating equation(10) from

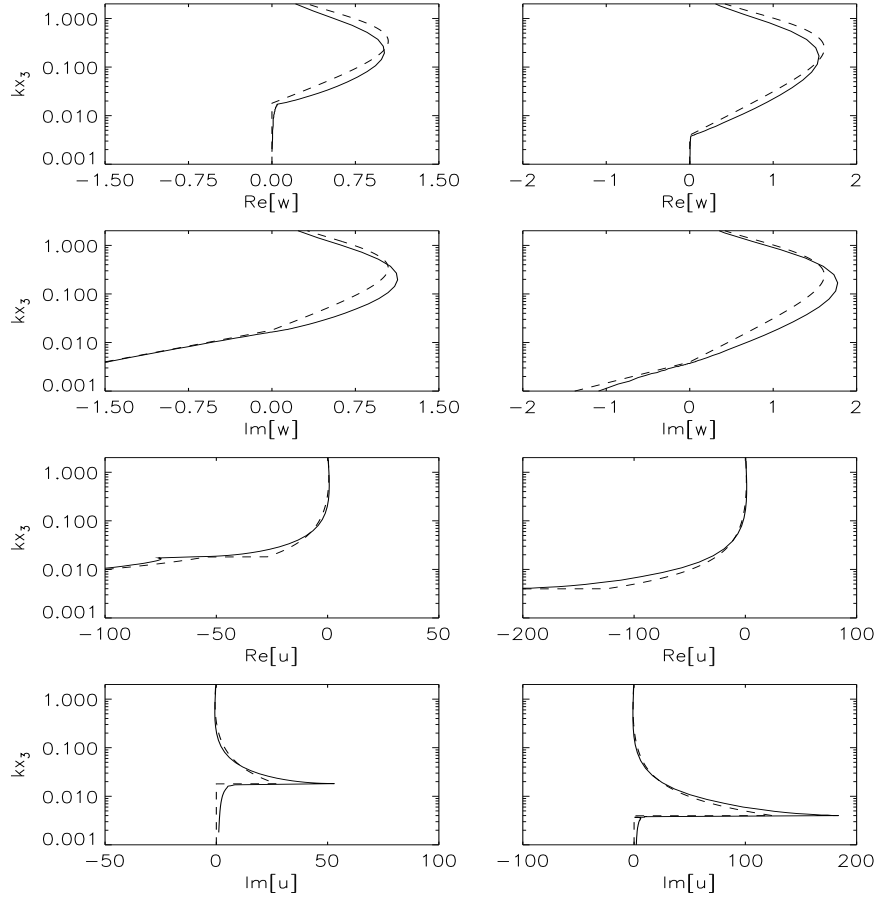


Figure 2. Inviscid shear flow: profiles of real and imaginary parts of vertical $\hat{w}(z)$ and horizontal $\hat{u}(z)$ velocities. The wind speed is $U_{10}=15 \text{ m s}^{-1}$. The inverse wave age parameter is $U_{10}/c = 2$ (left column), and $U_{10}/c = 5$ (right column). The approximate solution, equations (33) and (35), is shown by dashed lines. The solid lines show the numerical solution of the Rayleigh equation (27) with the horizontal velocity defined through the continuity equation (4). The velocities are normalized with $ak\bar{u}_*/\kappa$. The critical height is $kz_c=0.018$ for $U_{10}/c = 2$, and $kz_c=0.004$ for $U_{10}/c = 5$.

infinity to z_c , and substituting the obtained relation for the imaginary part of \hat{P} into equation (9)

$$\hat{w}_0(z_c) = \text{Re}(\gamma) \frac{\kappa k z_c}{u_*} \int_{z_c}^{\infty} U^2 e^{-kz} d(kz). \quad (31)$$

The approximate solution for the horizontal velocity can be obtained via \hat{w}_0 defined by (28) from the continuity equation. In Cartesian coordinates (x_1, x_3) the approximate solution for the horizontal velocity

reads

$$\hat{u}_0(x_3) = i\gamma \left[-U + k^{-1}U' \right] e^{-kx_3}. \quad (32)$$

This solution is shown in Figure 2 along with the numerical solution of the Rayleigh equation. The approximate solution for horizontal and vertical velocities compares reasonably well with the numerical solution. We shall apply the approximation of \hat{w}_0 (28) for the description of the outer region in the turbulent boundary layer.

3.1.2. Turbulent air flow

In Section 2.3 we argue that the singular behavior of the critical layer dynamics has to be significantly suppressed by turbulence. Therefore, we describe the vertical velocity in the OR by equation (28) where $\gamma = i$ throughout the whole wave boundary layer, i.e.

$$\hat{w}_0(z) = iU(z)e^{-kz}. \quad (33)$$

This solution describes the basic behavior of the vertical motion - its decay with height - in the turbulent wave boundary layer. It can be shown that the solution is correct only in zero-order. The Reynolds stresses inside the IR induce a vertical velocity which is of the kl -order (Belcher and Hunt, 1993). To obtain the solution of \hat{u}_0 with the same accuracy as \hat{w}_0 , we use the vorticity equation (19). In terms of normal modes this equation has the form

$$ikU \left(\frac{\partial \hat{u}_0}{\partial z} - ik\hat{w}_0 \right) + (\hat{w}_0 - ie^{-kz}U)U'' + ike^{-kz}UU' = 0. \quad (34)$$

Substituting (33) for \hat{w}_0 into the vorticity equation and integrating the obtained expression for $\partial \hat{u}_0 / \partial z$ from ∞ to z with the boundary condition $\hat{u}_0(\infty) = 0$, we obtain the following approximate solution for the horizontal velocity

$$\hat{u}_0(z) = Ue^{-kz} + 2 \int_z^\infty e^{-kz}U' dz. \quad (35)$$

Thus, the general feature of the wave-induced motion in the outer region is described by equations (33) and (35) for the vertical and the horizontal velocity respectively. This is the zero-order solution in the sense of expansion (26). The kl -correction of the solution for $\hat{u}_0(z)$ does not introduce new essential elements in the description of the horizontal velocity in the OR. However the kl -correction of the vertical velocity is important as $Re(\hat{w})$ determines the energy transfer from wind to waves and will be considered later.

3.2. INNER REGION

3.2.1. Reynolds stresses

In the IR the Reynolds stresses are in equilibrium with the local gradient of the wind velocity. Consequently, they can be described by the local eddy-viscosity closure scheme

$$\tau_{13} = K \left(\frac{\partial u}{\partial z} + \frac{\partial w}{\partial x} \right), \quad (36)$$

$$\tau_{23} = K \left(\frac{\partial v}{\partial z} + \frac{\partial w}{\partial y} \right). \quad (37)$$

Here K is the eddy-viscosity, which is expressed via the square root of the turbulence kinetic energy e and the turbulence length scale which is proportional to the distance from the surface

$$K = \kappa z e^{1/2}. \quad (38)$$

The normal Reynolds stresses in the IR are assumed to be proportional to the shear stress

$$\tau_{11} = -\alpha_u (\tau_{13}^2 + \tau_{23}^2)^{1/2}, \quad (39)$$

$$\tau_{33} = -\alpha_w (\tau_{13}^2 + \tau_{23}^2)^{1/2}, \quad (40)$$

where α_u and α_w are empirical constants. The shear stress can be found from the TKE conservation equation, in which a the local balance between the TKE production and its dissipation is assumed

$$\tau_{13} \frac{\partial u}{\partial z} + \tau_{23} \frac{\partial v}{\partial z} - \frac{e^{3/2}}{\kappa z} = 0. \quad (41)$$

Inside the IR, the wave-induced variation of the vertical gradient of the horizontal velocity is $(kl)^{-1}$ times larger than the variation of the horizontal gradient of the vertical velocity. In the kl -order, the linearized equation (41) written in terms of normal modes is

$$\widehat{K} \left[\left(\frac{\partial U}{\partial z} \right)^2 + \left(\frac{\partial V}{\partial z} \right)^2 \right] + 2\overline{K} \frac{\partial U}{\partial z} \frac{\partial \widehat{u}}{\partial z} - 3 \frac{\overline{K}^2 \widehat{K}}{\kappa^4 z^4} = 0. \quad (42)$$

The solution of this equation is

$$\widehat{K} = \kappa^2 z^2 \cos \theta \frac{\partial \widehat{u}}{\partial z}, \quad (43)$$

and the shear stress is derived from (36) and (43)

$$\begin{aligned} \widehat{\tau}_{13} &= \widehat{K} \frac{\partial U}{\partial z} + \overline{K} \frac{\partial \widehat{u}}{\partial z} \\ &= (1 + \cos^2 \theta) \kappa z \overline{u}_* \frac{\partial \widehat{u}}{\partial z}. \end{aligned} \quad (44)$$

This relation is valid well inside the IR (at $z < l$). According to rapid distortion theory, the shear stress attenuates towards the outer region. To take this effect into account we introduce a vertical damping of the shear stress and rewrite (44)

$$\hat{\tau}_{13} = (1 + \cos^2 \theta) \kappa z \bar{u}_* \frac{\partial \hat{u}}{\partial z} e^{-z/l}. \quad (45)$$

At small z/l this equation reduces to (44), while at large z/l the shear stress vanishes.

3.2.2. Vorticity equation in the IR

Let us introduce a new dimensionless vertical coordinate inside the IR:

$$\zeta = z/l, \quad (46)$$

and rewrite the vorticity equation (18) in terms of normal modes accounting for the shear and normal stresses (45), (39) and (40)

$$\begin{aligned} & iU \left(\frac{\partial \hat{u}}{\partial \zeta} - ikl\hat{w} \right) + (kl)^{-1} (\hat{w} - ie^{-kl\zeta}U) U''_{\zeta\zeta} + ie^{-kl\zeta}UU'_\zeta \\ &= \frac{1 + \cos^2 \theta}{2} \frac{\kappa |U_l|}{\bar{u}_*} \left[\frac{\partial^2}{\partial \zeta^2} + (kl)^2 - ikl \cos \theta (\alpha_u - \alpha_w) \frac{\partial}{\partial \zeta} \right] \left(\zeta e^{-\zeta} \frac{\partial \hat{u}}{\partial \zeta} \right) \end{aligned} \quad (47)$$

The continuity equation (11) in the ζ -coordinate reads

$$ikl\hat{u} + \frac{\partial \hat{w}}{\partial \zeta} - ie^{-kl\zeta}U'_\zeta = 0, \quad (48)$$

where $U'_\zeta = \partial U(\zeta)/\partial \zeta$ and $U''_{\zeta\zeta} = \partial^2 U(\zeta)/\partial \zeta^2$.

Figure 1 shows that the height of the IR kl is small except in a narrow range in the vicinity of $U_{10}/c \sim 1.2$. Outside this narrow range the terms of the kl - order can be neglected in equation (47), which then takes the form

$$\frac{1}{2}(1 + \cos^2 \theta) \frac{\partial^2}{\partial \zeta^2} \left(\zeta e^{-\zeta} \frac{\partial \hat{u}_0}{\partial \zeta} \right) - i \frac{\bar{u}_* U}{\kappa |U_l|} \frac{\partial \hat{u}_0}{\partial \zeta} = S(\zeta), \quad (49)$$

where the function $S(\zeta)$ is

$$\begin{aligned} S(\zeta) &= \frac{\bar{u}_*}{\kappa |U_l|} \left[\frac{(\hat{w} - ie^{-kl\zeta}U)U''_{\zeta\zeta}}{kl} + ie^{-kl\zeta}UU'_\zeta \right] \\ &= \frac{\bar{u}_*}{\kappa |U_l|} \left[\hat{w}_1 U''_{\zeta\zeta} + ie^{-kl\zeta}UU'_\zeta \right]. \end{aligned} \quad (50)$$

To obtain the second equality, the expansion (26) in powers of kl for the vertical velocity is used, so that \hat{w}_0 is defined by (33) and \hat{w}_1 is the

kl -order correction. The term S describes the source of vorticity caused by the vertical motion in the shear flow.

3.2.3. Solution of the problem: shear stress and horizontal velocity

It is more convenient to rewrite equation (49) in terms of the shear stress variation

$$\frac{\partial^2 \hat{\tau}_0}{\partial \zeta^2} - m^2(\zeta) \hat{\tau}_0 = S_0(\zeta), \quad (51)$$

where $\hat{\tau}_0 = 2\kappa \bar{u}_* \zeta e^{-\zeta} \partial \hat{u}_0 / \partial \zeta$ is the shear stress variation when $\theta = 0^0$, and $m^2(\zeta)$ is a function defined as

$$m^2(\zeta) = \frac{4i}{1 + \cos^2 \theta} \frac{\bar{u}_*^2 U e^\zeta}{|U_l| \zeta}. \quad (52)$$

The source of vorticity $S_0(\zeta)$ is

$$S_0(\zeta) = \frac{4\bar{u}_*^2}{(1 + \cos^2 \theta) |U_l|} \left(\hat{w}_1 U_{\zeta\zeta}'' + i e^{-kl\zeta} U U_\zeta' \right). \quad (53)$$

The kl -order correction of the vertical velocity can be found from the continuity equation (48) if the zero-order solution \hat{u}_0 for the horizontal velocity is known

$$\hat{w}_1(\zeta) = i \int_{\zeta_0}^{\zeta} (\hat{u}_0 - U e^{-kl\zeta}) d\zeta. \quad (54)$$

Equation (51) is an ordinary non-uniform differential equation of the second order with respect to the shear stress $\hat{\tau}_0$, or of the third order with respect to the horizontal velocity \hat{u} . The boundary conditions have to be specified. At the upper boundary of the IR, $\zeta = n$ (in the present study we adopt $n = 3$), the solution of the equation has to patch the horizontal velocity \hat{u}_n and its vertical gradient in the OR, i.e.

$$\hat{u}_0(n) = \hat{u}_n, \quad (55)$$

$$\hat{\tau}_0(n) = 2n e^{-n} \kappa \bar{u}_* \frac{\partial \hat{u}}{\partial \zeta} \Big|_{\zeta=n}. \quad (56)$$

At the lower boundary $\zeta = \zeta_0 \equiv z_0/l$, the solution of (51) has to patch the horizontal component $\hat{u}_s = \kappa c / \bar{u}_*$ of the orbital velocity of the surface wave

$$\hat{u}_0(\zeta_0) = \hat{u}_s. \quad (57)$$

Accounting for the boundary condition (57), the relation between the wave-induced variation of the shear stress $\hat{\tau}_0$ and the wind velocity \hat{u}_0 is

$$\hat{u}_0(\zeta) = \hat{u}_s + \frac{1}{2\kappa \bar{u}_*} \int_{\zeta_0}^{\zeta} \hat{\tau}_0(\zeta) e^\zeta d \ln \zeta. \quad (58)$$

At small ζ in the lower part of the IR the shear stress is approximately constant with height. Hence, the profile of the wind velocity variation according to (58) has a logarithmic shape. This thin sublayer adjacent to the surface is usually referred to as the inner surface layer (Belcher and Hunt, 1993). The magnitude of the shear stress at the surface $\hat{\tau}_0(\zeta_0)$ is unknown, and should be found so that the solution of equation (51) with the upper boundary condition (56) obeys the condition

$$\hat{u}_n - \hat{u}_s = \frac{1}{2\kappa\bar{u}_*} \int_{\zeta_0}^n \hat{\tau}_0(\zeta) e^{\zeta} d \ln \zeta. \quad (59)$$

Equation (51) (with (52), (53) and (54)) can be solved with the upper boundary (56) and integral condition (59) either analytically or numerically. In equation (51) the vorticity source S_0 depends on the kl -correction of the vertical velocity \hat{w}_1 in (54), which in turn depends on the solution of (51). An example of the analytical solution of the problem is given by Kudryavtsev et al. (1999). However, the simplest way to solve these coupled equations is to use an iterative method. The following procedure was applied: 1) The first guess for $\hat{\tau}_0$ at $\zeta = \zeta_0$ is taken. 2) Equation (51) with the upper boundary condition (56) and $\hat{\tau}_0(\zeta_0)$ is solved numerically. 3) The profile of the shear stress found is integrated over the IR according to the right hand side of (59). This results in an estimate of the horizontal velocity difference over the IR $\Delta\hat{u}_0$. 4) Depending on the difference between $\Delta\hat{u}_0$ and the true value $(\hat{u}_n - \hat{u}_s)$, $\hat{\tau}_0$ is corrected and the iteration is repeated from step (2). The iterations are continued until $|\Delta\hat{u}_0 - (\hat{u}_n - \hat{u}_s)| / |\hat{u}_n - \hat{u}_s|$ is small enough. Then $\hat{w}_1(\zeta)$ in (54) is updated with new \hat{u}_0 and the iteration starts again. The solution of equation (51) at arbitrary wind direction θ gives the vertical profile of the shear stress inside the IR

$$\hat{\tau}_{13}(\zeta) = \frac{1}{2}(1 + \cos^2 \theta)\hat{\tau}_0(\zeta), \quad (60)$$

and the profile of the horizontal velocity is found from (58).

3.2.4. Vertical velocity

The kl -order correction of the vertical velocity has an important physical meaning. It gives the real part of the vertical velocity, which determines the energy flux to waves. The vertical velocity correlated with the wave elevation produces the slope-correlated variation of the air pressure. The pressure correlated with the wave slope provides the energy transfer from the air flow to waves.

The first-order solution for the vertical velocity inside the IR follows from equation (54) with \hat{u}_0 defined by (58). However, this solution does not provide the attenuation of the vertical velocity above the IR. It is

clear that such a behavior of the vertical velocity is not physical, which is explained by the fact that the solution for \hat{u}_0 used in (54) is valid for small kz only, i.e. inside the IR. Outside the IR all wave-induced variables of the air flow decay exponentially with height. To account for this fact the exponential decay is introduced in equation (54), which then takes the form

$$\hat{w}_1(\zeta) = -ie^{-kl\zeta} \int_{\zeta_0}^{\zeta} (\hat{u}_0 - Ue^{-kl\zeta}) d\zeta. \quad (61)$$

Equation (61) helps to understand the mechanism of wave generation. The imaginary part of the horizontal velocity, produced by the action of the shear stress inside the IR, generates the real part of the vertical velocity, which is in phase with the wave elevation. This velocity penetrates into the inviscid OR and generates the slope-correlated pressure. The pressure then penetrates the thin IR and forms at the surface the energy flux from the air flow to the wave.

3.3. ENERGY TRANSFER FROM WIND TO WAVE

The growth of the wave energy E_w due to the energy transfer from wind to waves is described by equation

$$\frac{\partial E_w}{\partial t} = \rho_a c \left\langle P_s \frac{\partial \eta_0}{\partial x} \right\rangle + \rho_a \langle \tau_s u_s \rangle, \quad (62)$$

where $E_w = 1/2\rho_w g a^2$ is the energy of the gravity wave, ρ_a and ρ_w are the air and the water density, $P_s = P(z_0)$ is the surface pressure (including normal turbulent stresses), $\tau_s = \tau_{13}(z_0)$ is the surface shear stress, and brackets denote horizontal averaging over the wave length. The dimensionless growth rate parameter β is defined as

$$\beta = \frac{1}{E_w \omega} \frac{\partial E_w}{\partial t}. \quad (63)$$

In terms of normal modes (63) takes the form

$$\beta = \frac{\rho_a \bar{u}_*^2}{\rho_w c^2} \left[Im(\hat{P}_{0s}) + Re(\hat{\tau}_s) \right], \quad (64)$$

where $\hat{P}_{0s} = \hat{P}_0(\zeta_0)$, and $\hat{\tau}_s = \hat{\tau}_{13}(\zeta_0)$. The first term in (64) describes the energy flux due to the work of pressure on the vertical orbital velocity. The second term describes the work of the surface tangential stress on the horizontal orbital velocity. The surface pressure can be found from (10)

$$Im(\hat{P}_{0s}) = \kappa^{-2} k \int_{z_0}^{\infty} (U \hat{w}_{1r} - Re(\hat{\tau}_{13})) dz, \quad (65)$$

where the vertical velocity is defined by (61), and the shear stress is defined by (60).

4. Results

4.1. WIND VELOCITY AND SHEAR STRESS PROFILES

In this section we present a comparison of the wave-induced velocity and the Reynolds stress calculated by the simplified model (SWBL) with those calculated by the two-dimensional numerical wave boundary layer model (2D WBL). The 2D WBL model is described in detail by Mastenbroek et al. (1996). Here we only mention that the second-order Reynolds stress turbulence closure scheme developed by Launder et al. (1975) is used to model the turbulent stresses. A comparison is made for 4 cases specified by the parameters listed in Table 1. For the first 3 runs the direction of the wind coincides with the direction of the wave propagation; for run 4 the wave propagates against the wind. The vertical profiles of the velocity and the Reynolds stress are shown

Table I. Parameters of runs.

Run	U_{10}/c	c/u_*	kz_c	kl	kz_0
1	0.83	36.6	32.8	0.05	1.4×10^{-6}
2	1.66	18.3	8.5×10^{-2}	0.28	5.5×10^{-5}
3	5	6.1	5.7×10^{-3}	0.11	5.0×10^{-4}
4	1.5	15.9	-	0.03	5.6×10^{-5}

in Figures 3-6. Heights of the IR and the critical level are also shown in these figures.

In the outer region ($z > l$) the wave-induced motion is defined mainly by the elevation-correlated (real part) component of the horizontal velocity and the slope-correlated (imaginary part) component of the vertical velocity, which characterize the inviscid nature of the flow above the wavy surface. Their quadrature components ($Im(\hat{u})$ and $Re(\hat{w})$ respectively) are small. Notice, that in the OR the approximate solution by the SWBL model based on equations (33) and (35) is in an excellent agreement with the 2D WBL model for all 4 cases.

Run 1 (Figure 3) relates to waves in the vicinity of the spectral peak of a fully developed sea (inverse wave age $U_{10}/c = 0.83$). In this case

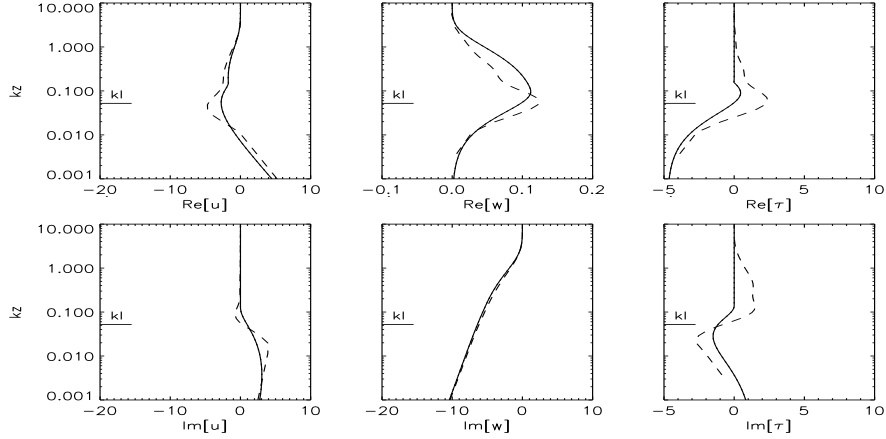


Figure 3. Profiles of real and imaginary parts of the horizontal velocity $\hat{u}(z)$, (left column), the vertical velocity $\hat{w}(z)$, (middle column), and the shear stress $\hat{\tau}(z)$ (right column). The solid lines show the solution of the simplified model; the dashed lines show the solution of the 2D WBL model. Inverse wave age is $U_{10}/c=0.83$. Wind velocities are normalized with $ak\bar{u}_*/\kappa$, and the shear stress is normalized with $ak\bar{u}_*^2$.

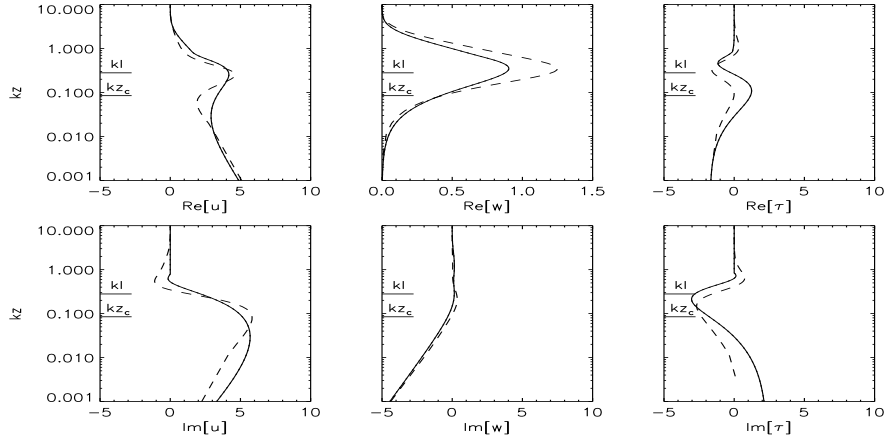


Figure 4. The same as in figure 3, but inverse wave age is $U_{10}/c=1.66$.

the critical height is located outside the wave boundary layer, so that the influence of the critical layer on the air flow dynamics is absent. The dynamics of the OR is mainly defined by the inviscid air flow undulations over the wave profile, while the structure of the IR is fully determined by the action of the shear stress. At the surface the stress provides the patching of the air flow velocities to the orbital velocities of the wave. This results in the generation of the slope-correlated horizontal velocity inside the IR, and hence, through the continuity

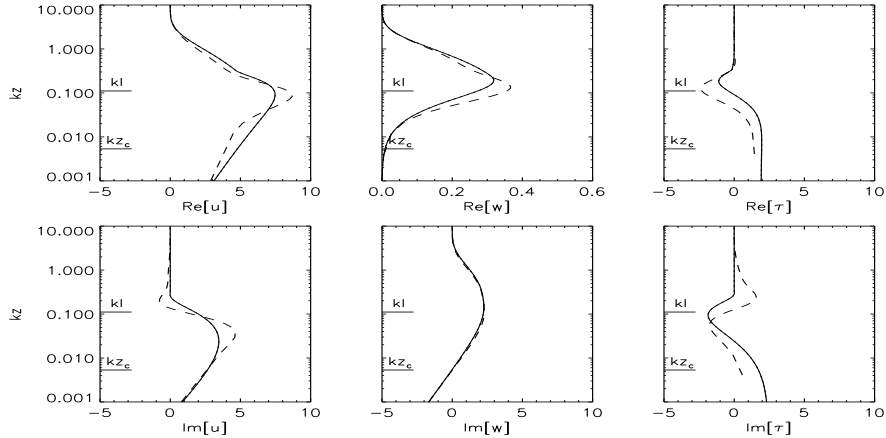


Figure 5. The same as in figure 3, but inverse wave age is $U_{10}/c=5$.

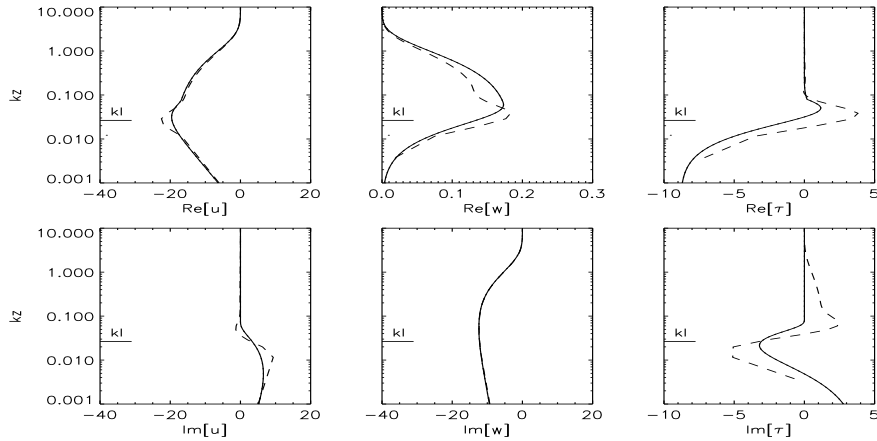


Figure 6. The same as in figure 3, but for the wave moving opposite the wind. Inverse wave age is $U_{10}/c=1.5$.

equation, the elevation-correlated component of the vertical velocity. The latter is of the kl -order and small but plays a crucial role in the energy exchange between wind and waves. The vertical profiles of the shear stress obtained by the simplified and the numerical models are in qualitative and quantitative agreement. Both models predict a strong enhancement of the surface stress in the region of the wave trough.

Run 2 (Figure 4) corresponds to a case when the frequency of the wave is twice the frequency of the spectral peak of a fully developed sea (inverse wave age is $U_{10}/c = 1.66$). In this case the height of the IR is $kl = 0.28$, which is close to its maximal value as follows from Figure 1. The height of the critical level is $kz_c = 0.085$. This is comparable

to the IR height, which could give rise to complication. The accuracy of our approximation is of the kl -order, and one could anticipate a significant deviation of the solution of the SWBL model from the 2D WBL model. However, the comparison is encouraging. The simplified model reproduces the local maximum in $Re(\hat{u})$ and the local minimum in the shear stress well, both occurring in the region of the critical layer. Notice, that as the critical layer is located inside the IR, the singular behavior of the air flow dynamics, which is well expressed in the left column of in Figure 2, is significantly blurred by turbulent stresses.

Run 3 (Figure 5) corresponds to a case of a slow wave (inverse wave age $U_{10}/c = 5$). Again a good comparison in the velocity distribution between the models is found. The structure of the IR is characterized by a speed-up of the horizontal velocity over the crest. Both models predict the maximum of the horizontal velocity (as well as the real part of the vertical velocity) in the vicinity of the IR height. The 2D WBL model gives a somewhat stronger acceleration of the flow than the simplified model. The vertical profile of the shear stress is in qualitative agreement, though the local extremum in $Re(\hat{\tau})$ seems to be underestimated by the simplified model. Furthermore, unlike the simplified model, the 2D WBL model predicts the existence of the slope-correlated stress $Im(\hat{\tau})$ in the OR. The critical layer for this run is located in the lower part of the IR, where the shear stress dominates the air flow dynamics, and there is no manifestation of the singular behavior of the air flow at the critical level.

Finally, run 4 (Figure 6) corresponds to a case of swell propagating against the wind. In this case the minimum of the horizontal velocity occurs over the trough of the wave. Inside the IR the action of the shear stress shifts the region of the accelerated air flow to the downwind slope. The maximum of the stress is in the vicinity of the wave trough. Again, the simplified description of the turbulent wave boundary layer is well consistent with the one obtained by 2D WBL model.

The comparison of the results shows, that the simplified model correctly reproduces the general peculiarities of the air flow dynamics over surface waves in a wide range of wind-wave conditions as compared to the 2D WBL model.

4.2. GROWTH RATE PARAMETER

In Figure 7, a comparison of the growth rate parameter resulting from the simplified and the 2D WBL models is shown. In the IR the air flow dynamics is governed mainly by the shear stress. The stress generates the real part of the vertical velocity in the kl -order (61), which in turn generates the slope-correlated surface pressure (65), providing the

energy transfer from wind to wave. This is the so-called non-separated sheltering wave growth mechanism described by Belcher and Hunt (1993).

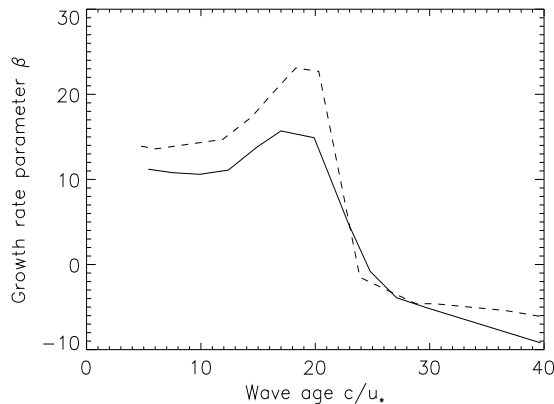


Figure 7. The growth rate parameter as a function of c/\bar{u}_* . The solid line denotes the solution of the simplified model; the dashed line denotes the solution of the 2D WBL model.

Qualitatively, the simplified model reproduces well the growth rate dependence on wave age c/u_* resulting from the 2D WBL model. Quantitatively, the SWBL model gives somewhat lower values of β . This is explained by the fact that the simplified model predicts a smaller magnitude of the vertical velocity $Re(\hat{w}_1)$ and hence $Im(\hat{P}_{0s})$ than that predicted by the 2D WBL model. In the range $15 < c/u_* < 22$ the growth rate parameter has a peak. Its origin can be explained by the fact that the critical height here approaches the upper boundary of the IR, and peculiarities of the critical layer dynamics, though still suppressed by weakened turbulence, become important. In the range of fast waves the growth rate parameter is negative, which means that the energy flux is from the wave to the air flow.

4.3. COMPARISON WITH MEASUREMENTS

In this section results of the simplified and the 2D WBL models are compared with the laboratory measurements of velocity and stress fields by Hsu and Hsu (1983). They used a mechanically generated wave with phase velocity $c = 1.6 \text{ m s}^{-1}$. Other parameters of three runs of this experiment are shown in Table 2. U_∞ is the wind speed in the centre of the tank, $u_{* \text{exp}}$ is the friction velocity presented by Hsu and Hsu. The wind velocity at $z = k^{-1} U(k^{-1})$ and the friction velocity u_*

Table II. Parameters of runs of the experiment by Hsu and Hsu (1983)

Run	U_∞	$u_{* \text{ exp}}$	$U(k^{-1})$	u_*	$U(k^{-1})/c$
	(m/s)	(m/s)	(m/s)	(m/s)	
1	1.37	0.043	1.4	0.06	0.87
2	2.12	0.073	2.0	0.08	1.28
3	2.92	0.110	2.9	0.13	1.84

are determined by fitting the logarithmic profile to the observed mean wind speed.

The wave-induced horizontal velocity and the shear stress measured in the wave following coordinate system are shown in Figures 8-10. The vertical velocity is not shown in the figures as there is an apparent bias in these data of which the cause is unknown (Mastenbroek, 1996).

Runs 1 and 2 relate to cases when the wave moves somewhat slower and faster than the wind respectively; run 3 represents a slowly propagating wave. In cases 1 and 3 the measurements were done in both outer and inner regions, while in case 2 the IR depth is large, and most of data are confined to the inner region. The data confirm the existence of the outer and the inner regions. For case 1 nor 2 no significant variation of the shear stress is observed inside the OR, while inside the IR a systematic trend in the shear stress is clearly seen. In run 2 the IR is high, and the stress varies throughout the whole domain. Peculiarities of the wave-induced horizontal velocity are dependent on the ratio of the wind speed to the wave phase velocity. If the wave runs faster than the wind, then the air flow accelerates over the trough (run 1). Otherwise, the air flow accelerates over the crest (run 2 and 3): the larger the speed difference between wind and wave, the stronger the acceleration.

The simplified model reproduces the behavior of the wave-induced disturbances of velocity and stress fields above the wave well. The only significant deviation of the model predictions from the data can be observed in the lower part of the vertical profile of $Im(\hat{\tau})$ the reason of which is not understood. However, the 2D WBL model suffers the same deficiency. In fact, it is not possible to judge which of the two models behaves better as compared to measurements.

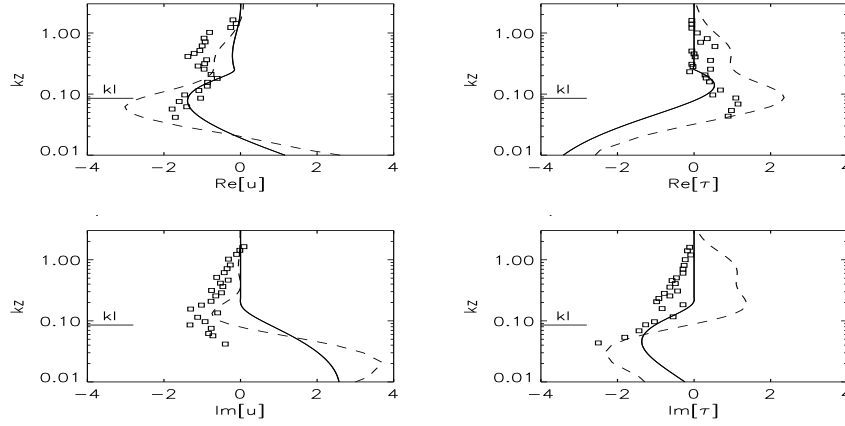


Figure 8. Comparison of simplified model (solid lines), and 2D WBL model (dashed lines) with laboratory measurements of Hsu and Hsu (1983) (open squares). Run 1: $U_k=1.4\text{m s}^{-1}$; $U_k/c=0.87$ (see Table 2 for details). The horizontal velocity is normalized with $ak\bar{u}_*/\kappa$, and the shear stress is normalized with $ak\bar{u}_*^2$

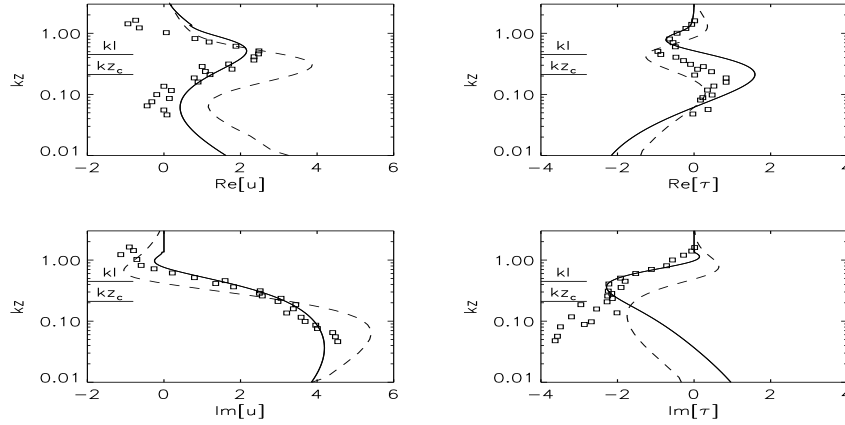


Figure 9. The same as in figure 8, but for run 2: $U_k=2.0\text{m s}^{-1}$; $U_k/c=1.28$.

5. Discussion and Conclusions

A simplified model of the wave boundary layer over a surface wave propagating at an arbitrary phase velocity and direction as compared to the wind vector is presented. The main simplification of the problem is achieved by the division of the wave boundary layer into the outer (OR) and the inner (IR) regions, as suggested by Belcher and Hunt (1993). In the OR the wave-induced motion experiences inviscid undulation,

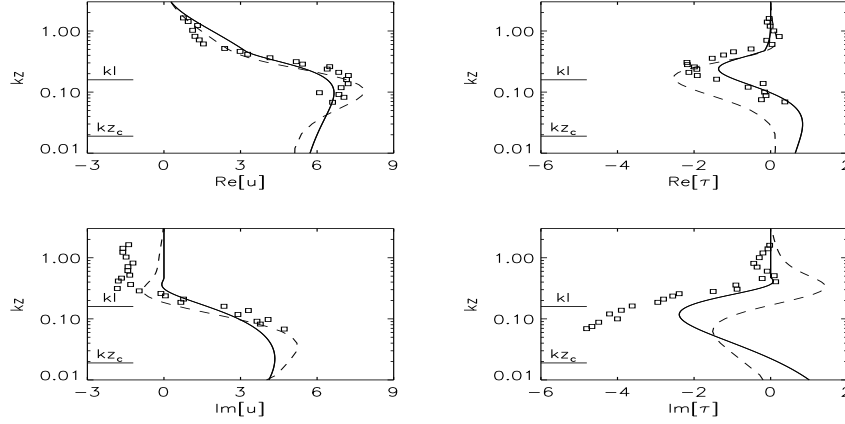


Figure 10. The same as in figure 8, but for run 3: $U_k=2.9\text{m s}^{-1}$; $U_k/c=1.84$.

while in the IR the motion is strongly affected by the turbulent shear stress.

The IR depth is relatively small ($kl \sim 0.1$) for all waves, except for those running with a phase speed close to the wind velocity (i.e. the inverse wave age parameter is $1 < U_{10}/c < 1.2$). In this narrow range the height of the IR is $kl \sim 1$. An important conclusion resulting from the analysis of the IR depth is that the critical height (the height where the wind speed equals the phase velocity of the wave) is almost always located inside the IR. This means that the singular behavior of the critical layer dynamics is strongly suppressed by the turbulent stress for all waves, with exception of those with inverse wave age $U_{10}/c \approx 1.2$.

The fact that the singular behavior of the critical layer dynamics does not influence the inviscid outer region allows a simple description of the velocity in the OR. This description is based on the approximate solution of the Rayleigh equation suggested by Miles (1957). The solution for the vertical velocity is proportional to the mean wind velocity and an exponential decay function. The approximate solution for the horizontal velocity results from the integration of the inviscid vorticity equation with the known vertical velocity. The description of the OR in the simplified model is presented by explicit formulas, and is compared with the numerical solution of the Rayleigh equation. A good comparison is found.

The description of the IR is based on the solution of the vorticity conservation equation which accounts for the turbulent diffusion of the vorticity. The turbulent shear stress is parameterized using the mixing length closure theory. Introduction of exponential vertical damping of the wave-induced shear stress leads to a further simplification of the

problem. The damping of the shear stress describes phenomenologically the basic feature of the wave boundary layer: the rapid distortion of turbulence in the OR. The zero-order solution (in terms of a kl -power expansion) of the vorticity equation can be found either numerically or analytically. An example of the analytical solution of the problem is given in Kudryavtsev et al. (1999). In the present study the vorticity equation is solved numerically.

Correction of the IR solution in the kl -order has a physical significance only for the real part of the vertical velocity. This component of the vertical motion, being generated inside the IR due to the action of the shear stress, penetrates into the OR and generates the slope-correlated component of the air pressure. The pressure penetrates into the thin IR and forms the energy and momentum flux between wind and waves (the non-separated sheltering mechanism of wave generation by Belcher and Hunt (1993)).

The comparison of results obtained by the simplified and the 2D WBL models is encouraging. A reasonable agreement is found for the wave-induced velocity, the shear stress and the growth rate parameter. This fact has a very important consequence: the description of the air flow dynamics over waves appears to be not very sensitive to the details of the turbulence closure scheme used. For a correct description of the air flow the scheme has to provide the vertical damping of the wave-induced stress at a scale comparable with the IR height. The phenomenological approach used in this paper is based on the direct suppression of the turbulent stress with height. This gives results which are in good agreement with those found by using the second order Reynolds stress closure scheme.

The results of the simplified model are consistent with data of Hsu and Hsu (1983) obtained in a laboratory experiment. The experimental data confirm the existence of the outer and the inner region above waves.

Acknowledgements

For V.K. and V.M. this research was supported by the Office of Naval Research (ONR Grant Number N00014-98-1-0437, and N00014-98-1-0653, PR number 98PR04572-00, and 98PR05889-00), and by EU Environment Programme (Contract ENV4-CT97-0460, ASPEN). J.F.M. was supported by the Netherlands Organization for Scientific Research. V.K. would like to thank the staff of Modelling and Application Division and Oceanographic Division for their hospitality during his visits to KNMI as a guest researcher. Our pleasure to acknowledge Dr. Gerbrand

Komen for numerous helpful discussions, and for providing us with the code for the numerical solution of the Rayleigh equation.

References

- Belcher, S.E. and Hunt, J.C.R.: 1993, 'Turbulent shear flow over slowly moving waves', *J. Fluid Mech.* **251**, 109-148.
- Belcher, S.E. and Hunt, J.C.R.: 1998, 'Turbulent flow over hills and waves', *Annu. Rev. Fluid Mech.* **30**, 507-538.
- Cohen, J.E.: 1997, *Theory of turbulent wind over fast and slow waves*. PhD Thesis, Univ. Cambridge, 228 pp.
- Harris, J.A., Belcher, S.E. and Street, R.L.: 1996, 'Linear dynamics of wind waves in coupled turbulent air-water flow: Part 2', *J. Fluid Mech.* **308**, 219-254.
- Hsu, C.T. and Hsu, Y.: 1983, 'On the structure of turbulent flow over a progressive water wave: theory and experiment in a transformed, wave-following coordinate system. Part 2.', *J. Fluid Mech.* **131**, 123-153.
- Komen, G.J., Cavaleri, L., Donelan, M., Hasselmann, K., Hasselmann, S. and Janssen, P.A.E.M.: 1994, *Dynamics and modelling of ocean waves*, Cambridge Univ. Press, 540p.
- Kudryavtsev, V.N., Mastenbroek, C. and Makin, V.K.: 1997, 'Modulation of wind ripples by long surface waves via the air flow: A feedback mechanism', *Boundary-Layer Meteor.* **83**, 99-116.
- Kudryavtsev, V.N., Makin, V.K. and Meirink, J.F.: 1999, *Turbulent air flow over sea waves: simplified model for applications*, KNMI Scientific Report, WR 99-02, KNMI, De Bilt, 37 pp.
- Launder, B.E., Reece, G.J. and Rodi, W.: 1975, 'Progress in the development of a Reynolds-stress turbulence closure', *J. Fluid Mech.* **16**, 138-159.
- Lighthill, M.J.: 1957, 'The fundamental solution for small steady three-dimensional disturbances to a two-dimensional parallel shear flow', *J. Fluid Mech.* **3**, 1-13.
- Mastenbroek, C., Makin, V.K., Garat, M.H. and Giovanangeli, J.P.: 1996, 'Experimental evidence of the rapid distortion of turbulence in the air flow over water waves', *J. Fluid Mech.* **318**, 273-302.
- Mastenbroek, C.: 1996, *Wind-Wave Interaction*, Ph.D. thesis, Univ. of Delft, Delft, Netherlands, 119 pp.
- Mestayer, P.G., van Eijk, A.M.J., de Leeuw, G. and Tranchant, B.: 1996, 'Numerical simulation of the dynamics of sea spray over the waves', *J. Geophys. Res.*, **104**, 20771-20797.
- Miles, J.W.: 1957, 'On the generation of surface waves by shear flow', *J. Fluid Mech.* **3**, 185-204.
- Miles, J.W.: 1959, 'On the generation of surface waves by shear flows. Part 2', *J. Fluid Mech.* **6**, 568-582.
- Phillips, O.M.: 1966, *The dynamics of the upper ocean*, Cambridge Univ. Press, 261 pp.